Journal of Hazardous Materials 164 (2009) 600–608

Contents lists available at ScienceDirect

Journal of Hazardous Materials

journal homepage: www.elsevier.com/locate/jhazmat

Effect of filler types and calcination temperature on the microstructure and the nitric oxide photocatalytic activity of composite titanium dioxide films

Haiqiang Wang, Zhongbiao Wu*, Yue Liu

Department of Environmental Engineering, Zhejiang University, Zhe Da Road, No. 38, Hangzhou 310027, Zhejiang, PR China

ARTICLE INFO

Article history:
Received 29 April 2008
Received in revised form 13 August 2008
Accepted 13 August 2008
Available online 20 August 2008

Keywords:
Photocatalysis
NO
Composite TiO_2 film
Sol–gel
Photocatalytic oxidation

ABSTRACT

The composite titanium dioxide (TiO_2) films coating on the woven glass fabric were prepared by a modified sol–gel process, using pre-calcinated TiO_2 nanoparticle or silica gel as filler. The characterized physicochemical properties of the prepared catalyst films showed that the specific surface area, the microstructure and the crystal structure of the catalysts were greatly affected by the fillers and the calcination temperature. The physicochemical properties of composite films and the photocatalytic activity of nitric oxide (NO) show that the pre-calcinated TiO_2 nanoparticle is more favorable than silica gel as filler. The pre-calcinated TiO_2 nanoparticle filler can increase the photocatalytic activities of the catalysts by increasing the specific surface area, introducing a bimodal mesoporous structure, and creating a polymorphous crystal structure. And the TiO_2-TiO_2 film calcinated at 400 °C exhibits the highest photocatalytic activity for NO oxidation and is more active than Degussa P25.

1. Introduction

Nitrogen oxides (NO_x), such as nitric oxide (NO), nitrous oxide (N_2O) and nitrogen dioxide (NO_2) emitted from industrial boilers, internal combustion furnaces and engines are one kind of harmful atmospheric pollutants which can cause acid rain, photochemical smog and greenhouse effects. Various processes, including combustion modifications, dry processes and wet processes have been developed to remove NO from flue gas [1]. Wet processes are very efficient to remove NO_2 from flue gas, but cannot remove NO because of its low solubility in aqueous solution. One promising approach to improving the absorption efficiency of wet processes is the oxidation of NO to NO_2 by photocatalytic oxidation (PCO) in gas-phase [2–5].

The photocatalytic decomposition of NO_x in the ambient atmosphere, using titanium dioxide (TiO_2) as the photocatalyst, was firstly reported in 1994 [6]. Ichiura et al. studied the photocatalytic decomposition of nitrogen oxides over titanium dioxide sheets that contained metal compounds [7]. Dalton et al. investigated the NO_x adsorbate reaction on the TiO_2 substrate surface in the photocatalytic reaction [8]. Hashimoto et al. reported the photocatalytic decomposition of NO with Hycom TiO_2 and zeolite to remove NO_x in the atmosphere [9]. Recently, group of Lee had done a series of excellent studies of the NO photocatalytic decomposition in the indoor air conditions, including the relation between NO and other pollutants and the improved method for the catalyst preparation [10–16].

The PCO of NO was first reported by Devahasdin et al. [17], but the PCO efficiency of NO in his experiment was low. Therefore, it is still necessary to develop more effective ways to enhance the oxidation efficiency of NO. Also, developing an immobilized photocatalyst is needed for the practical industrial application [18–22].

For the photocatalytic oxidation of NO, the photocatalyst must first provide abundant adsorption site for NO. Secondly, nitrogen dioxide must desorb immediately from the photocatalyst surface which was a marked difference compared with the common photocatalytic decomposition of air pollutants (VOCs) [17,23,24].

Producing immobilized TiO_2 films for future industrial applications has gained a lot of attentions in the past years. Sol–gel process was one of the most common methods [19,20], and glass materials just like glass substrate, glass fabric and woven glass fabric were usually used as catalyst support. However, the immobilized films produced by common sol–gel methods exhibit relatively low photocatalytic activity because of their low surface area and small film thickness. To improve the physical properties of TiO_2 films, the application of filler in the sol–gel process was studied widely. Recently, it has been demonstrated that the addition of pre-calcinated TiO_2 particle (Degussa P25) could improve the film surface structure and the film thickness greatly [25–31]. Hence, it could enhance the performances of catalysts. However, the influences of the filler types have received little attention. Furthermore,

* Corresponding author. Tel.: +86 571 87952459; fax: +86 571 87953088.
E-mail address: zbwu@zju.edu.cn (Z. Wu).

0304-3894/$ – see front matter © 2008 Elsevier B.V. All rights reserved.
doi:10.1016/j.jhazmat.2008.08.035

few of the studies were focused on the photocatalytic oxidation of nitric oxide.

In this study, several TiO_2-based photocatalyst films (using woven glass fabric as support) were prepared by a modified sol–gel process using pre-calcinated TiO_2 nanoparticle or silica gel powder as the filler. Their capabilities for NO oxidation were evaluated in the presence of air under UV-light irradiation. The physicochemical properties of the prepared TiO_2 catalysts were fully characterized and the effects of filler types and calcination temperature on the physical properties of the catalysts were investigated. Finally, the relationship between the physical properties and NO oxidation efficiency of the catalysts were discussed.

2. Experimental

2.1. Material

NO gas from a compressed gas cylinder with a nitrogen balance was used for the NO oxidation experiments (concentration: 10 000 ppm). The Degussa P25 TiO_2 powder was purchased from Degussa (crystal size: 20–50 nm, surface area: $50 \pm 5\ m^2\ g^{-1}$, crystal distribution: 70% anatase and 30% rutile). The silica gel powder was analytically pure (particle size: 2–5 μm). The woven glass fabric was supplied by Hangzhou woven glass fabric factory (thickness: 0.5 mm; filament diameter: 9 μm).

2.2. Preparation of TiO_2 catalysts

Tetrabutyl titanate (0.1 mol), acetic acid (0.3 mol), and anhydrous ethanol (0.5 mol) were mixed for 30 min using a magnetic stirrer. A solution of anhydrous ethanol (0.5 mol), acetic acid (0.3 mol) and distilled water (0.3 mol) was also prepared. The tetrabutyl titanate solution was added drop-wise into the above mixture under vigorous stirring. A clear titania sol was produced and the mixture was stirred at room temperature for 3 h. The obtained titania sol was used as precursor sol, and the pure TiO_2 films were prepared by this precursor sol.

Pre-calcinated TiO_2 powders (Degussa P25, ratio of powders:tetrabutyl titanate = 1:1), and silica gel powders (ratio of powders:tetrabutyl titanate = 1:1) were used as fillers, mixed with the precursor sol, for the coating samples. The powders were ultrasonically dispersed in the sol for 30 min.

All of the pristine woven glass fabrics were heated in an electric furnace at 500 °C for 1 h prior for immobilization of the TiO_2 ($4\ cm \times 80\ cm$, total surface area: $640\ cm^2$). This treatment ensured complete removal of organic impurities on the surface of the supports. Immobilization was carried out by the dip-coating method. The prepared TiO_2 sol or the powder-sol mixture was dip-coated onto the woven glass fabric and then dried at 100 °C for 1 h in an oven. The procedure was repeated 3 times, and the woven glass fabric was then dried at 100 °C for 24 h. Calcination was carried out at different temperatures (300–600 °C), in air, for 1 h. The typical catalyst loading achieved with this approach was $1.0\ mg/cm^2$. The bare TiO_2 film (Degussa P25) was also prepared by this dip-coating process without the treatment of calcination, the catalysts loading was approximately $1.0\ mg/cm^2$. In this experiment, the TiO_2 films were named as TF1, TF2, TF3 and TF4 with the different calcination temperatures respectively (300, 400, 500 and 600 °C). For TiO_2-TiO_2 films, they were named as TTF1, TTF2, TTF3 and TTF4 respectively (300, 400, 500 and 600 °C). For silica gel-TiO_2 films, they were named as STF1, STF2, STF3 and STF4 respectively (300, 400, 500 and 600 °C).

2.3. Characterization of TiO_2 catalysts

X-ray diffraction (XRD) analysis was performed on a Phillips diffractometer at 40 kV and 36 mA (Cu Kα = 1.542 Å), at an angle of 2θ from 10° to 80°. The scan speed was 1°/min. The strongest TiO_2 peaks, corresponding to anatase (1 0 1) and rutile (1 1 0), were selected to evaluate the crystal size of the samples. The mean crystal size was determined by the Scherer equation. Microstructures of the prepared samples, after being coated with gold, were observed with a scanning electron micrograph (SEM) Phillips XL-30-ESEM, at a voltage of 20 kV. The morphology, structure and grain size of TiO_2 particles were examined by transmission electron microscopy (TEM) and high resolution-transmission electron microscopy (HR-TEM) using a JEM-2010 instrument. The Brunauer–Emmett–Teller surface area (BET) of the powders was analyzed by a Micromeritics ASAP 2010C nitrogen adsorption apparatus (USA). Desorption isotherm was used to determine the pore distribution via the Barret–Joyner–Halender (BJH) method. Temperature programmed desorption (TPD) was carried out on a custom-made TCD setup using 100 mg catalysts. For NO-TPD or NO_2-TPD experiments, after pretreated in He at 400 °C for 1 h, catalysts were saturated with anhydrous NO or anhydrous NO_2 (4% in He) at a flow rate of 30 ml/min for about 30 min. Desorption was carried out by heating the sample in He (30 ml/min) from 100 to 800 °C with a heating rate of 5 °C/min.

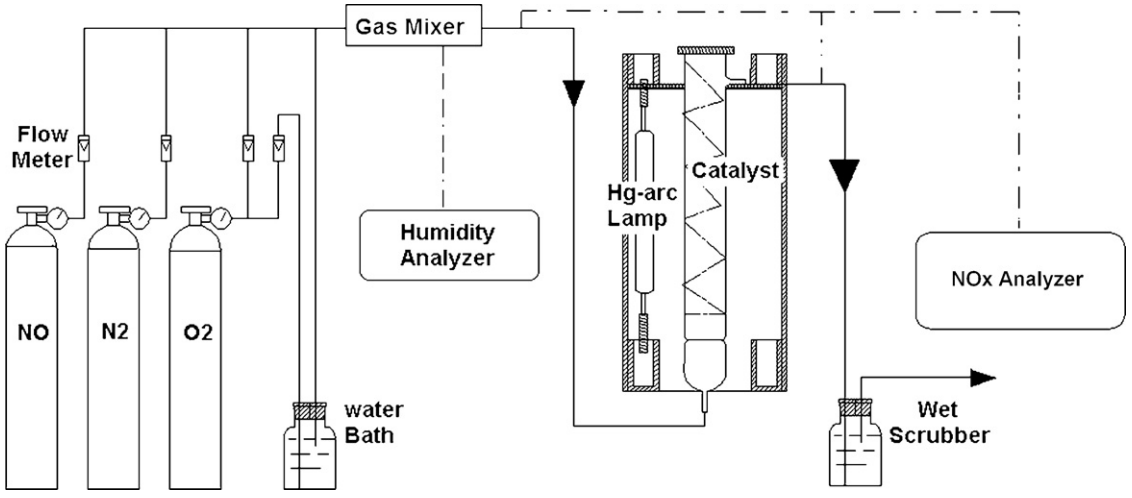

Fig. 1. Schematic diagram of the photocatalytic oxidation equipment.

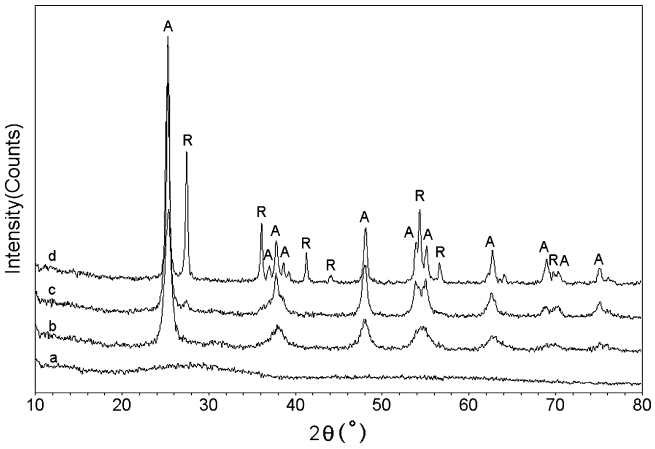

Fig. 2. XRD patterns of TiO_2 films under different calcination treatments: (a) TF1; (b) TF2; (c) TF3; (d) TF4.

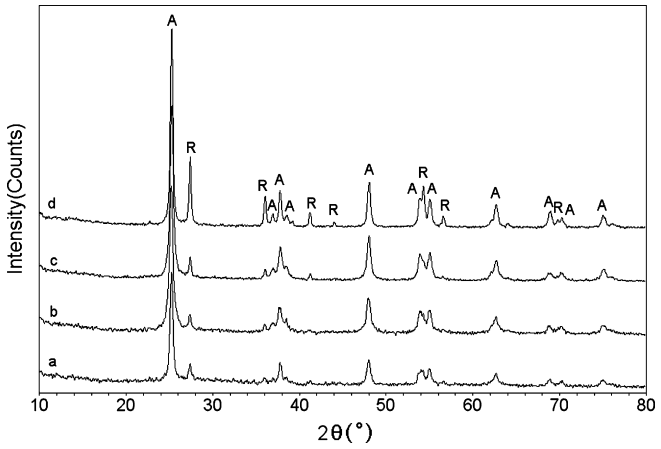

Fig. 3. XRD patterns of TiO_2-TiO_2 films under different calcination treatments: (a) TTF1; (b) TTF2; (c) TTF3; (d) TTF4.

2.4. Experimental setup

The schematic experimental setup is shown in Fig. 1, including the gas supply, PCO reactor, and analytical system. The air, NO, and N_2 gas streams were mixed to obtain the desired concentration and to adjust space time. The simulated flue gas used in the experiment was ca. 90 ppm NO_x (ca. 80 ppm NO), the flow rate of simulated flue gas was 2.0 l/min and the empty bed retention time (EBRT) was 10 s.

The immobilized catalyst was set into a 340 ml Pyrex reactor with "Z" type. The reactor was irradiated with an Hg-arc lamp (125 W, Philips) whose wavelength ranged from 300 to 400 nm with the maximum light intensity at 365 nm. The reactor and light source were set in a hollow chamber that was coated with tinfoil. The temperature of the reactor was lowered by the cooling gas (80 ± 5 °C). NO, NO_2 and O_2 were measured with a Kane International Limited Model KM-9106 flue gas analyzer. The relative humidity was measured with a Testo Co. Ltd. Model 605-H1 relative humidity analyzer.

The blank test consisted of a gas stream of ca. 90 ppm NO_x (ca. 80 ppm NO) that was irradiated by the Hg-arc lamp, without the TiO_2 photocatalyst. The variation in the NO concentration was not observed after 120 min of irradiation. Moreover, there was also no change of the NO concentration in the inlet or the outlet when the Hg-arc lamp was turned off while the catalyst was present in the reactor. Therefore, it is concluded that the absence of the TiO_2 or the Hg-arc lamp does not cause the oxidation of NO.

3. Results and discussion

3.1. Crystal structure and size of TiO_2 catalysts

The XRD patterns of the sol–gel TiO_2 catalyst films calcinated at different heat treatments are presented in Fig. 2. The crystal size of these catalysts, determining by the Scherrer equation, is between 0 and 33.6 nm, as listed in Table 1. As shown in Fig. 2, the TiO_2 film treated at 300 °C has an amorphous (and/or an ultra-fine crystalline) structure and exhibits a broad peak at about $2\theta = 25°$. By increasing the calcination temperature, the (1 0 1) anatase peak becomes sharper, which illustrates the dependence of crystallinity on the applied temperature. The phase transformation from anatase to rutile occurs around 500 °C. The maximum temperature used for samples preparation in this study was 600 °C, and at this temperature the percentage of rutile in the catalyst reached 38.9%.

The XRD patterns of the TiO_2-TiO_2 catalyst films calcinated at different heat treatments are presented in Fig. 3. As shown in Fig. 3, the (1 0 1) peak of anatase and the (1 1 0) peak of rutile appear when the calcination temperature is as low as 300 °C, mainly because pre-calcinated TiO_2 powders (Degussa P25) were used as filler. For the composite TiO_2-TiO_2 films, the initial anatase crystallite size increases only slightly with an increase in temperature, from 18.6 nm calcinated at 300 °C to 21.3 nm at 600 °C.

However, for the composite silica gel-TiO_2 films (Fig. 4), the crystallization behavior is similar to that of pure TiO_2 films. With this

Table 1
Characterization of the photocatalysts

Material	Code	Calcination temperature (°C)	Anatase (%)	Crystallite size (nm)	Rutile (%)	Crystallite size (nm)	Surface area ($m^2\ g^{-1}$)
TiO_2	TF1	300	–	–	–	–	–
film	TF2	400	100	9.7	–	–	83.5
	TF3	500	95.4	13.4	4.6	14.1	17.98
	TF4	600	61.1	21.1	38.9	32.6	2.46
TiO_2-	TTF1	300	84.9	18.6	15.1	19.0	115.4
TiO_2	TTF2	400	90.2	12.8	9.8	18.1	90.0
film	TTF3	500	88.1	16.3	11.9	25.6	58.5
	TTF4	600	69.8	21.3	30.2	33.6	26.6
Silica	STF1	300	100	3.0	–	–	340.8
gel-	STF2	400	100	8.2	–	–	264.3
TiO_2	STF3	500	100	10.9	–	–	210.0
film	STF4	600	79.0	17.0	21.0	27.4	177.5
Degussa P25	–	–		20–30		40–50	40–50

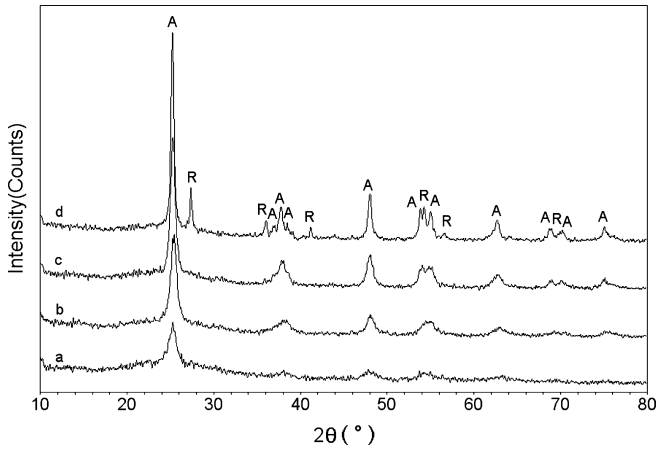

Fig. 4. XRD patterns of silica gel-TiO_2 films under different calcination treatments: (a) STF1; (b) STF2; (c) STF3; (d) STF4.

filler, the phase transformation from anatase to rutile takes place around 600 °C. This temperature is higher than that observed for pure TiO_2 films. As shown in Table 1, the anatase crystal size was decreased comparing with the TiO_2 films or TiO_2-TiO_2 composite films.

3.2. Surface morphology of TiO_2 catalysts

The morphology of the different catalyst films was examined by SEM and shown in Fig. 5. The surface of pure TiO_2 film is flat, and clear crack can be seen on the film. It is a compact film after the calcination process (Fig. 5a). For TiO_2-TiO_2 composite film (Fig. 5b), the surface is rough and the structure is complex. Obviously the addition of pre-calcinated TiO_2 particles retains the gel structure during drying and calcination. Degussa P25 particles and TiO_2 particles combine well in the catalyst surface. With the participation of pre-calcinated TiO_2 particle, a self-supported membrane or granule was produced [26]. Also it creates a mesoporous structures on the TiO_2-TiO_2 film surface. For the silica gel-TiO_2 film, lots of cracks appear on the film surface. But the TiO_2 films and silica gel particles are separated.

Fig. 6 shows HRTEM images of TiO_2 films, TiO_2-TiO_2 films and silica gel-TiO_2 films prepared by the sol–gel process. From the HRTEM micrograph of TiO_2 film (Fig. 6a), it can be seen that the primary particle size is about 10 nm, which is in agreement with the value of the crystallite size determined by XRD (9.7 nm, as shown in Table 1). Furthermore, it can be found that the TiO_2 particles on the TiO_2 films have a good crystallinity and these particles have a compact structure together. For the composed TiO_2-TiO_2 films (Fig. 6b), the large particles (20–50 nm) are the pre-calcinated TiO_2 particles which have a perfect crystallinity and a clear fringe, and the little particles dispersed around the large particles are generated from the TiO_2 sol. The addition of pre-calcinated TiO_2 particles inhibits the growth of TiO_2 particles (from the sol) in some degree and provides a polymorphous crystal structure of TiO_2. Furthermore, the pre-calcinated TiO_2 particles and the generated TiO_2 particles are combining well together. Also, one can see lots of slits on the composite TiO_2 films, due to the stereospecific blockade of pre-calcinated TiO_2 particles. For the composed silica gel-TiO_2 films (Fig. 6c), the crystal size of TiO_2 particles is about 8 nm, and little of the TiO_2 particle is coated on the silica gel surface. The addition of silica gel also inhibits the growth of TiO_2 particles (from the sol), but the filler (silica gel) and the catalyst is separate which is unlike the structure of composite TiO_2-TiO_2 films.

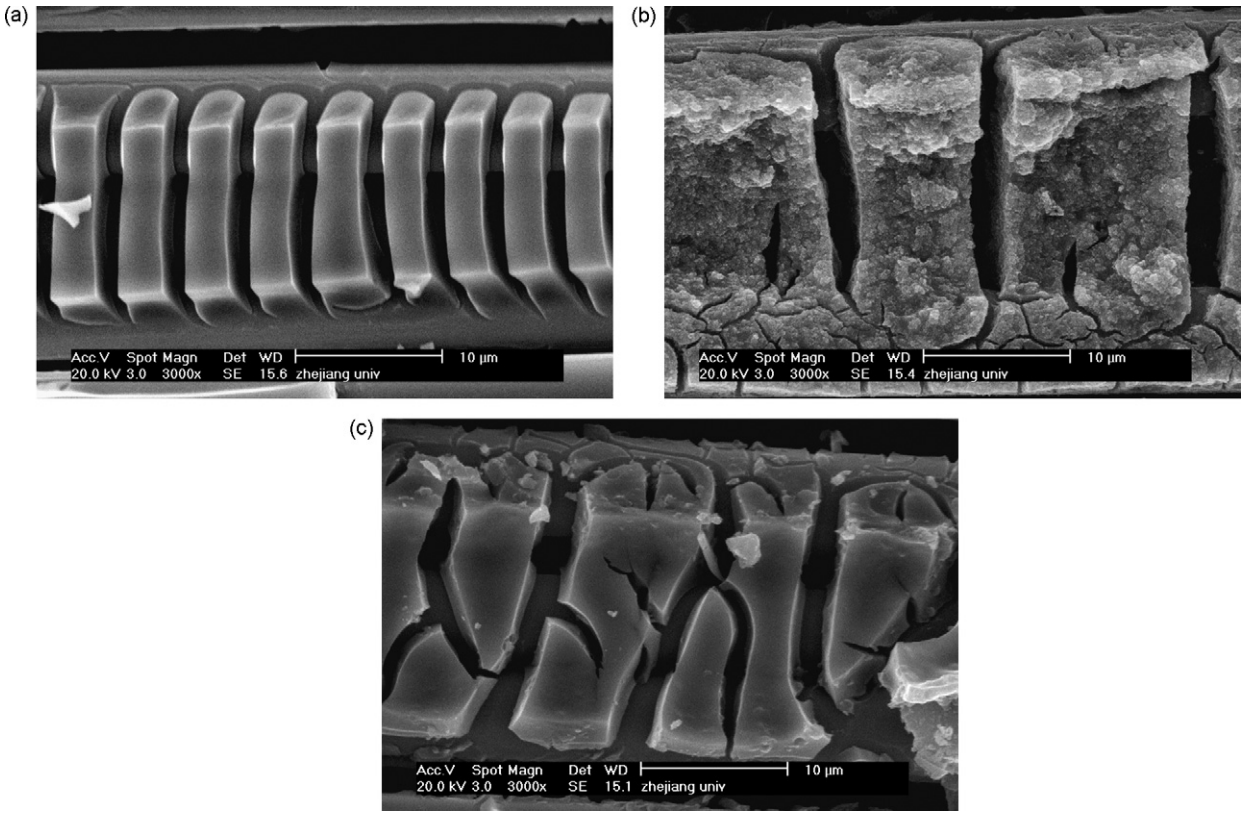

Fig. 5. SEM images of surface morphologies of the TiO_2 films and the composite TiO_2 films support on woven glass fabric: (a) TF2, 3000×; (b) TTF2, 3000×; (c) STF2, 3000×.

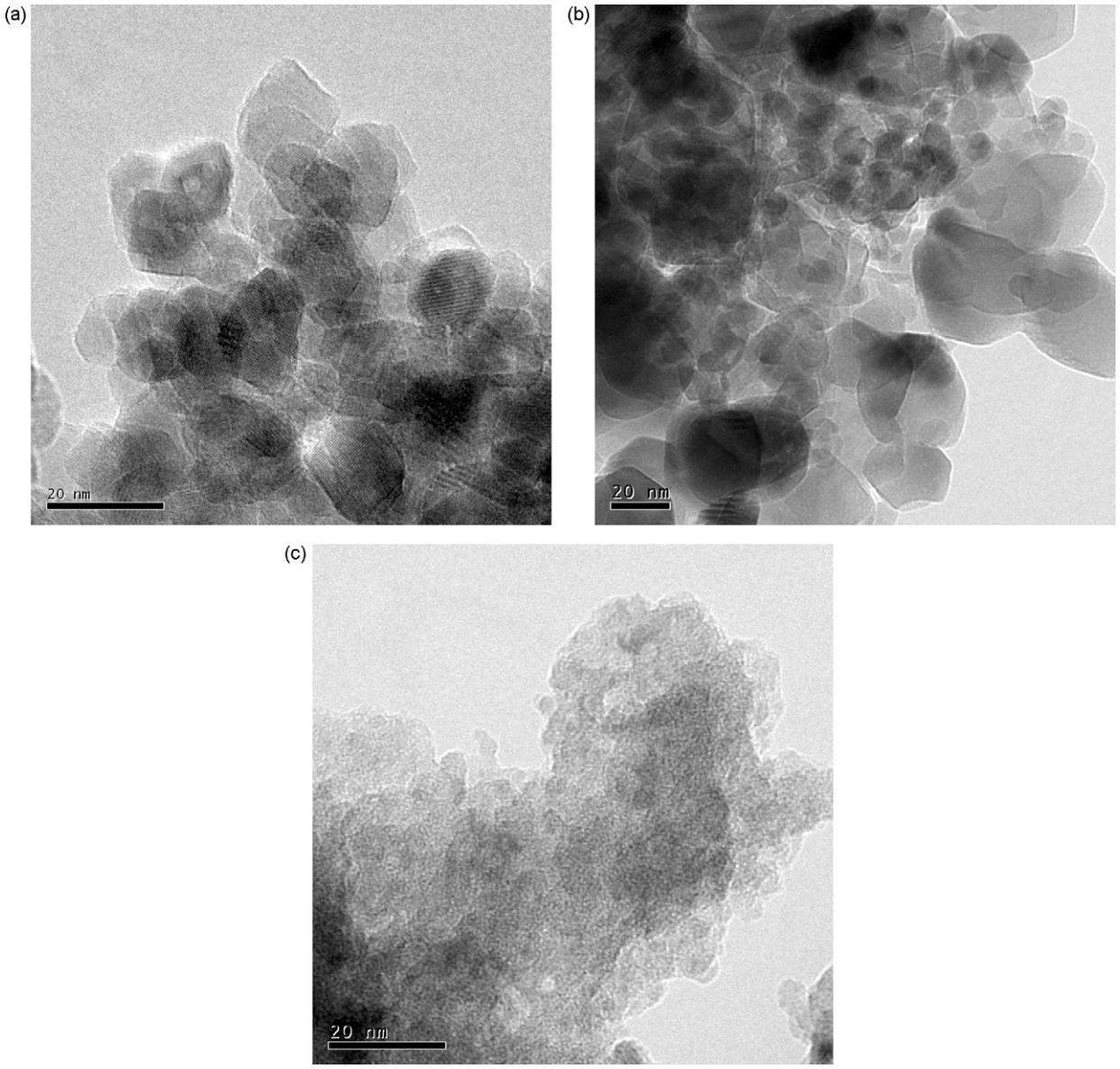

Fig. 6. TEM images of the TiO_2 films and the composite TiO_2 films support with fiberglass: (a) TF2; (b) TTF2; (c) STF2.

3.3. BET surface and pore distribution of catalysts

The analytical results for the TiO_2 films, the composite TiO_2-TiO_2 films and the composite silica gel-TiO_2 films are listed in Table 1. The BET data in Table 1 shows that addition of the filler in the TiO_2 sol can increase the surface area of catalyst films greatly. When the calcination temperature is 400 °C, the BET surface area of the TiO_2 film is 83.5 $m^2\ g^{-1}$. While for the TiO_2-TiO_2 film and silica gel-TiO_2 film, the surface areas are 90.0 and 264.3 $m^2\ g^{-1}$ respectively. Using silica gel as filler can increase the surface area three times as the TiO_2 films. Furthermore, the surface area of pure TiO_2 film declines dramatically with the increase of calcination temperature. But with the addition of fillers, the surface area of the composite films decreases tardily.

In order to investigate the effect of filler types on the pore structure of the prepared films, the above samples were analyzed by N_2 adsorption, and the results are shown in Figs. 7–9. The inserted adsorption isotherms in Figs. 7–9 show that all of the films presented type IV isotherms, indicating the presence of mesopores (2–50 nm) [32]. As for the pure TiO_2 films (Fig. 7), the observed hys-

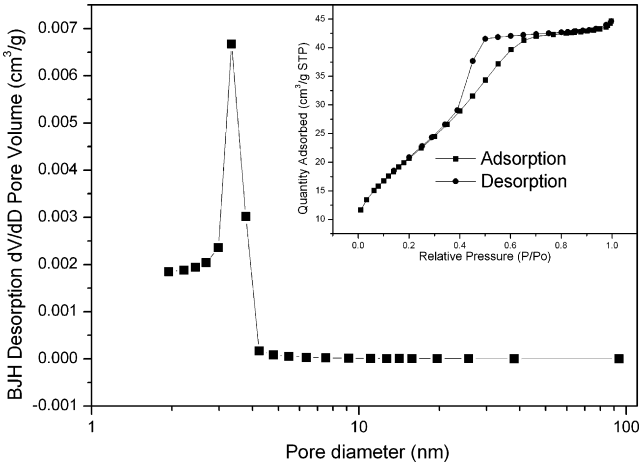

Fig. 7. Pore-size distributions of pure TiO_2 film (TF2).

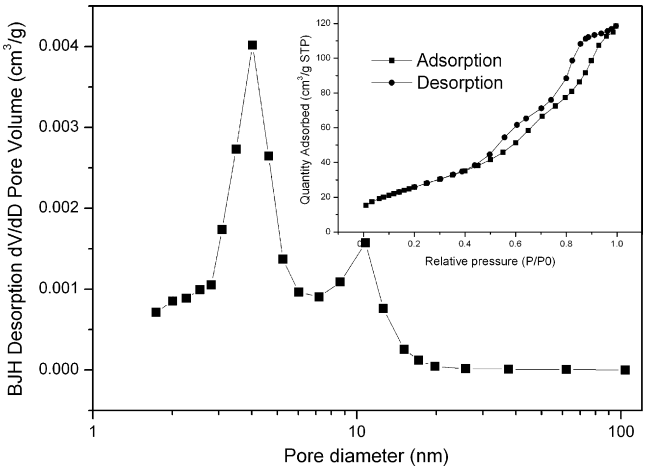

Fig. 8. Pore-size distributions of composite TiO_2-TiO_2 film (TTF2).

teresis loop is a type of H2 at lower relative pressure. The pore-size distribution of TiO_2 film is narrow (2.5–4.2 nm). With the addition of pre-calcinated TiO_2 particles, the hysteresis loop of the TiO_2-TiO_2 composite film is a mixture type of H2 at lower relative pressure and H3 at higher relative pressure. The hysteresis loop at lower relative pressure region ($0.4 < P/P_0 < 0.8$) is attributed to smaller mesopore, while that at higher relative pressure ($0.8 < P/P_0 < 1.0$) is attributed to larger mesopores [31]. Fig. 8 shows that TiO_2-TiO_2 film has the pore size of ~4 and ~13 nm with the maximum pore volume. It was found that using pre-calcinated TiO_2 as filler cannot only lead to an enhancement in the BET surface area of the films, but also to an evolution of pore structure from mono-modal pore-size distribution to bimodal pore-size distribution. However, the hysteresis loop of the silica gel-TiO_2 composite film is a mixture type of H1 and H2 at lower relative pressure. Fig. 9 shows that the main pore volume of silica gel-TiO_2 film is micropore volume (<2 nm) and the quantity of mesopore volume is a little in the composite silica gel-TiO_2 film.

3.4. Adsorption and desorption performances of catalysts

The adsorption and desorption performances of the catalysts were determined by NO and NO_2 temperature programmed desorption measurements, and the results are shown in Fig. 10.

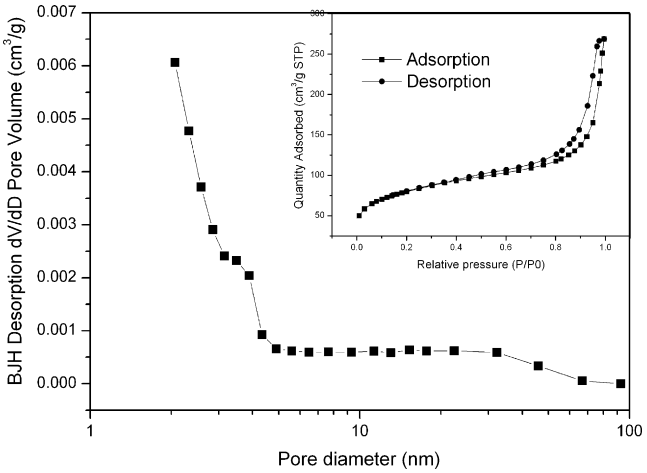

Fig. 9. Pore-size distributions of composite silica gel-TiO_2 film (STF2).

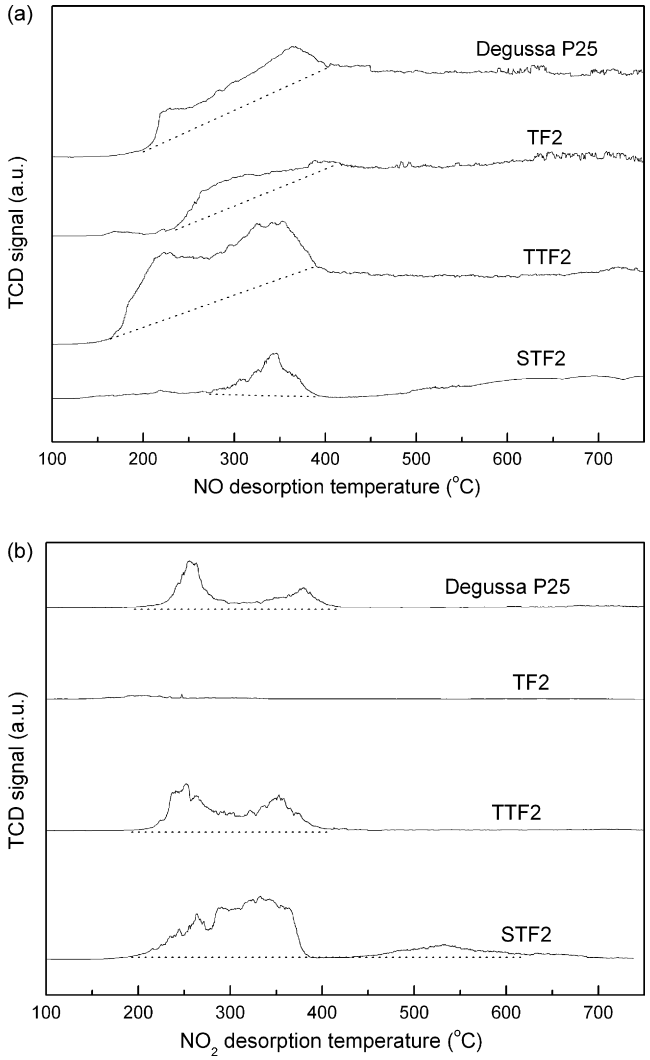

Fig. 10. NO-TPD and NO_2-TPD profiles for various catalysts: (a) NO-TPD; (b) NO_2-TPD.

From the NO-TPD curves of pure Degussa P25 and TF2, it is observed that one broad desorption peak spanned in the temperature range of 200–400 °C is present for both samples which is attributed to NO desorbed form the catalysts (Fig. 10a). While the peak area of Degussa P25 is larger than that of TF2. With the modification of P25 powder, the NO desorption peak area of TTF2 enlarge greatly. For the silica-gel modified catalyst (STF2), the NO desorption peak area has a little increase and the desorption temperature is ranged from 275 to 400 °C. From the NO_2-TPD curves for the catalysts (Fig. 10b), two peaks spanned in the temperature range of 200–400 °C are observed for the Degussa P25 and no desorption peak is present for the TF2. These two peaks are also measured for the TTF2 sample and the peak areas have little change. But the NO_2 adsorption and desorption behaviors are changed a lot with the modification of silica gel. One broad peak ranged from 200 to 400 °C and another peak ranged from 450 to 600 °C are observed for the STF2 sample.

Obviously, with the modification of Degussa P25, the NO adsorption capability is improved greatly and the NO_2 adsorption capability is scarcely influenced for the composite titania film. But with the modification of silica gel, the NO adsorption capability increases a little and the NO_2 adsorption capability increases greatly for the composite titania film.

3.5. Test of NO photocatalytic activity

Removal of NO from a gaseous phase was carried out in a continuous-flow reactor using different catalysts. The gas stream of ca. 90 ppm NO_x (ca. 80 ppm NO) in air (relative humidity: 60–70%; O_2 concentration: 21%) passed through the reactor at a flow rate of 2.0 l/min with an empty bed retention time of 10 s. After a stabilized period of about 1 h, outlet NO concentration became the same as that of inlet gas and then the experiment was started by turning on the UV lamp.

The concentrations of NO and NO_2 were recorded by the NO_x analyzer. A typical experimental result of NO and NO_2 concentrations against the reaction time (use Degussa P25 as catalyst) is shown in Fig. 11. At the start time, the concentration of NO dropped rapidly, and then after 30 min a steady state was achieved. During the steady state, the concentration of NO and NO_2 are kept as constant in the experiment. The NO oxidation efficiency is evaluated according to the definition of NO conversion = (([NO]inlet − [NO]outlet)/[NO]inlet) × 100. The PCO efficiency of NO by Degussa P25 was 48.8% at the steady time.

The PCO behavior of NO has already been studied by Devahasdin et al. [17]. The PCO behavior consists of a series of oxidation steps: $NO \rightarrow HNO_2 \rightarrow NO_2 \rightarrow HNO_3$. At the initial stage of the reactions, NO is quickly adsorbed onto the catalyst and reacts with the hydroxyl radical to form nitrous acid (HNO_2). The adsorbed HNO_2 can further react with another hydroxyl radical to produce adsorbed NO_2. Furthermore the adsorbed NO_2 can be oxidized to produce HNO_3. When the equilibrium between HNO_2, NO_2 and HNO_3 is established on the catalyst, the feed NO will only be converted to NO_2. Thus NO_2 is the dominant product at the steady state. The photocatalyst used in their work

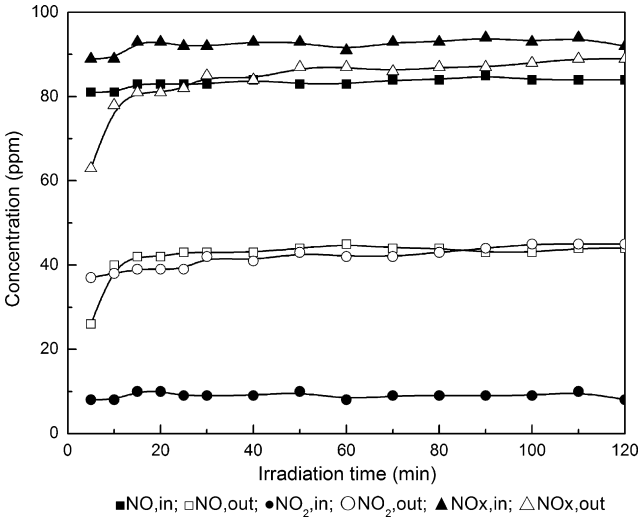

Fig. 11. The variation of NO, NO_2 and NO_x concentration with the irradiation time (catalyst: Degussa P25, dip-coating on woven glass fabric).

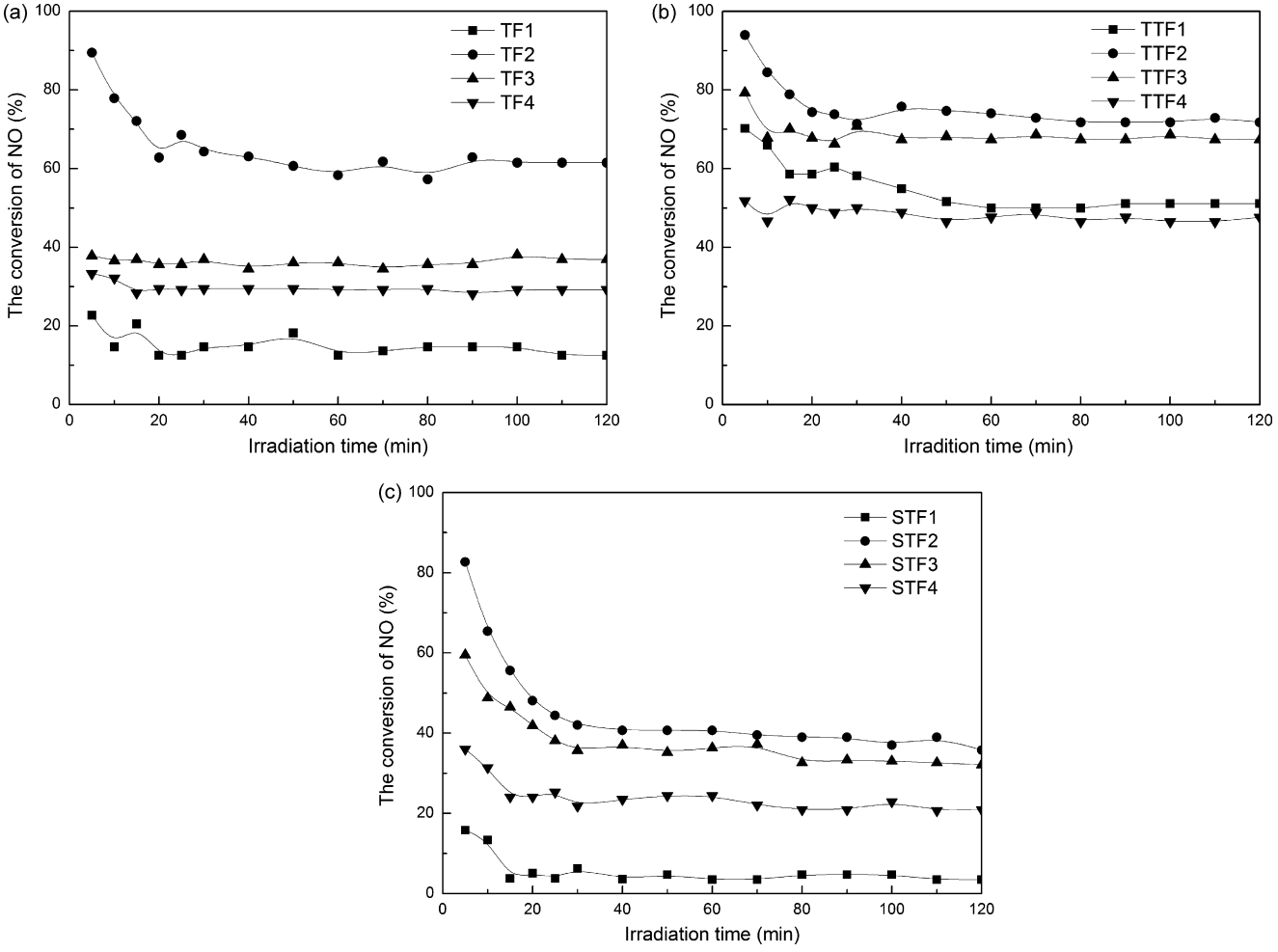

Fig. 12. The photocatalytic oxidation efficiency of difference TiO_2 films: (a) pure TiO_2 films; (b) composite TiO_2-TiO_2 films; (c) composite silica gel-TiO_2 films.

was also Degussa P25, and the PCO efficiency was nearly 30% (inlet NO: 40 ppm, space time: 12 s, UV-light: 2×25 W black light).

For the catalysts of TF1, TF2, TF3 and TF4, the conversion of NO is 14.7, 61.5, 36.9 and 29.2% respectively at the steady state (Fig. 12a). The activity of catalyst varies with the calcination temperature. When the calcination temperature is 300 °C, the NO photocatalytic activity is very low because of the low crystallinity of TiO_2 particles which is also approved by the XRD patterns (Fig. 2). The TF2 TiO_2 film has the best NO photocatalytic activity among the pure TiO_2 films. Above this calcination temperature, the crystal size of the TiO_2 film increases and the surface area declines with the increasing calcination temperature, leading to the decline of NO photocatalytic activity.

The conversion of NO for the catalysts of TTF1, TTF2, TTF3, and TTF4 at steady state is shown in Fig. 12b. This illustrates that the TiO_2 nanoparticle filler can significantly improve the activity of the catalysts. It is clear that TTF2 exhibits the highest photocatalytic activity for NO conversion and is more active than Degussa P25. In addition, the conversion of NO for the composite silica gel-TiO_2 films is shown in Fig. 12c. The results indicate that the NO photocatalytic activities of composite silica gel-TiO_2 films are all declining and the silica gel is not a favorable filler for composite TiO_2 films.

3.6. Discussion

The photocatalytic activity of TiO_2 photocatalyst is governed by many factors, such as: (a) crystal structure, (b) surface area and (c) pore structure.

Anatase and rutile are the most studied phases among the three crystal phases of TiO_2. Anatase is generally considered to be the active component based on the comparison between anatase and rutile [33]. However, a lot of literature reports that mix-phase TiO_2 (anatase and rutile) had the better photocatalytic activity than pure anatase and rutile [34–36]. The hole and electron can transfer between anatase and rutile because of their different valence band and conduction band, which successfully separate the photogenerated electron–hole pairs. Also, many catalytic "hot spots" may be located at the solid-solid interface of anatase and rutile, which is favorable for the improvement of photocatalytic activity [33]. Besides, the crystal size of catalyst particles and surface area are also important factors for the photocatalytic activity. For the pure mesoporous TiO_2 films, the anatase structure is formed when the calcination temperature is higher than 400 °C. Calcinated at 500 °C, the pure mesoporous TiO_2 film becomes a mixture crystal of anatase and rutile (Fig. 2). Its surface area is decreased and the crystal size is increased (Table 1). Thus, the TF2 film with pure anatase structure, larger surface area and smaller crystal size has the best photocatalytic oxidation efficiency among the pure mesoporous TiO_2 films. With the addition of pre-calcinated TiO_2 particles, the crystal structure is changed under the lower calcination temperature (300 °C). TiO_2 particles generated from TiO_2 sol have not been crystallized under this calcination temperature. With the increasing calcination temperature, the composition of TiO_2 crystal is redistributed in the composite TiO_2-TiO_2 films. The crystal size of anatase in TTF2 declines with the increasing calcination temperature because of the formation of the little anatase crystal generated from the TiO_2 sol. The addition of silica gel inhibits the augmentation of anatase crystal size and the formation of rutile structure (Fig. 4, Table 1). Calcinated at 400 °C, the crystal size of anatase is only 8.2 nm. The rutile structure did not form before 600 °C. In the aspect of crystal structure, the pre-calcinated TiO_2 particles (Degussa P25) are better than silica gel to use as fillers.

For the photocatalytic oxidation of nitric oxide, the main product of reaction is nitrogen dioxide. To ensure the steady progress of the reaction, nitrogen dioxide should desorb from the catalyst surface immediately, which is a marked difference between the photocatalytic oxidation of nitric oxide and the common photocatalytic decomposition of air pollutants (VOCs). Hence, the pore structure of the photocatalyst which is the key factor in the adsorption–desorption process should play more part in the process of NO photocatalytic oxidation. With the traditional sol–gel process, the pure TiO_2 film coated on the woven glass fabric is a typical mesoporous film with a narrow pore distribution (~3.8 nm, Fig. 7). The adsorption capability of NO and NO_2 are low (Fig. 10). After the modification of pre-calcinated TiO_2 particles, the surface area of the composite TiO_2-TiO_2 film is enhanced and the pore structure is transferred to a bimodal pore-size distribution from a mono-modal pore-size distribution. While the NO adsorption capability is increased and the NO_2 adsorption capability is scarcely influenced for the TiO_2-TiO_2 film (Fig. 10). When the silica gel is used as the filler, the main pore volume of silica gel-TiO_2 film is the micropore volume (pore size <2 nm). The great increase in BET surface area (Table 1) is due to the micropores in the composite silica gel-TiO_2 film. The NO adsorption capability increased a little and the NO_2 adsorption capability increased greatly for the silica gel-TiO_2 film (Fig. 10). Nitrogen dioxide is easy to adsorb on the zeolite or silica gel with micropore structure [37]. To desorb the nitrogen dioxide from these films, the enlarged pore size is favorable (Fig. 10). Hence, the composite TiO_2-TiO_2 film with bimodal pore-size distribution favors the adsorption of nitric oxide and the desorption of nitrogen dioxide from the photocatalyst surface compared with other films. At the steady state, nitrogen balance between the gas inlet and the gas outlet is built with the composite TiO_2-TiO_2 films. Thus the accumulation rate of products on the composite TiO_2-TiO_2 films can be neglected. In the experiments, it was also found that nitrogen balance was not built with the composite silica gel-TiO_2 films. The nitrogen dioxide concentration is reduced in the gas outlet, indicating that an excess amount of NO_2 was adsorbed on the surface of the silica gel-TiO_2 catalyst films. The nitrate ion could occupy the reaction site and decrease the NO photocatalytic activity.

From these observations, the addition of pre-calcinated TiO_2 particles in the TiO_2 sol can improve the crystal structure of TiO_2 at low calcination temperature, build a bimodal pore-size distribution and increase the surface area of the photocatalyst. The bimodal mesoporous TiO_2-TiO_2 film under 400 °C calcination temperature has the best photocatalytic oxidation efficiency among the tested TiO_2 films.

4. Conclusion

Photocatalytic oxidation of NO in air conditioning was investigated using several types of composite TiO_2 films in this study. The composite TiO_2 film coating on the woven glass fabric was prepared by a modified sol–gel process, using commercial TiO_2 nanoparticle or silica gel as filler.

The experiments demonstrate that the pre-calcinated TiO_2 nanoparticle is more favorable than silica gel as filler. It can increase the photo-efficiency of the catalysts by increasing the specific surface area, introducing a polymorphous structure under low calcination temperature, and building a bimodal pore-size distribution. Because of the favorable adsorption of NO_2, the nitrate ion may occupy the reaction site on the silica gel-TiO_2 films and that will decrease the photocatalytic efficiency of the silica gel-TiO_2 films as the reaction time increases. It is clearly shown that the composite TiO_2-TiO_2 film treated at 400 °C exhibits the highest photo-activity for NO oxidation and is more active than Degussa P25.

Acknowledgements

This project was financially supported by the National High-Tech Research and Development Program (863) of China (2007AA061701) and the New Century Excellent Scholar Program of Ministry of Education of China (NCET-04-0549).

References

[1] M. Radojevic, Environ. Poll. 102 (1998) 685–689.
[2] A.L. Linsebigler, G. Lu, J.T. Yates Jr., Chem. Rev. 95 (1995) 735–758.
[3] A. Fujishima, T.N. Rao, D.A. Tryk, J. Photochem. Photobiol. C: Photochem. Rev. 1 (2000) 1–21.
[4] G. Li, X.S. Zhao, M.B. Ray, Sep. Purif. Technol. 55 (2007) 91–97.
[5] A. Pal, S.O. Pehkonen, L.E. Yu, M.B. Ray, J. Photochem. Photobiol. A: Chem. 186 (2007) 335–341.
[6] T. Ibusuki, K. Takeuchi, J. Mol. Catal. 88 (1994) 93–102.
[7] H. Ichiura, T. Kitaoka, H. Tanaka, Chemosphere 51 (2003) 855–860.
[8] J.S. Dalton, P.A. Janes, N.G. Jones, J.A. Nicholson, K.R. Hallam, G.C. Allen, Environ. Poll. 120 (2002) 415–422.
[9] K. Hashimoto, K. Wasada, M. Osaki, E. Shono, K. Adachi, N. Toukai, H. Kominami, Y. Kera, Appl. Catal. B: Environ. 30 (2002) 429–436.
[10] C.H. Ao, S.C. Lee, C.L. Mak, L.Y. Chan, Appl. Catal. B: Environ. 42 (2003) 119–129.
[11] C.H. Ao, S.C. Lee, J.C. Yu, J. Photochem. Photobiol. A: Chem. 156 (2003) 171–177.
[12] C.H. Ao, S.C. Lee, Appl. Catal. B: Environ. 44 (2003) 191–205.
[13] C.H. Ao, S.C. Lee, J. Photochem. Photobiol. A: Chem. 161 (2004) 131–140.
[14] C.H. Ao, S.C. Lee, S.C. Zou, C.L. Mak, Appl. Catal. B: Environ. 49 (2004) 187–193.
[15] C.H. Ao, S.C. Lee, J.Z. Yu, J.H. Xu, Appl. Catal. B: Environ. 54 (2004) 41–50.
[16] F.B. Li, X.Z. Li, C.H. Ao, M.F. Hou, S.C. Lee, Appl. Catal. B: Environ. 54 (2004) 275–283.
[17] S. Devahasdin, C. Fan Jr., K. Li, D.H. Chen, J. Photochem. Photobiol. A: Chem. 156 (2003) 161–170.
[18] S. Gelover, P. Mondragón, A. Jiménez, J. Photochem. Photobiol. A: Chem. 165 (2004) 241–246.
[19] T. Wen, J.P. Gao, J.Y. Shen, Z.S. Zhou, J. Mater. Sci. 36 (2001) 5923–5926.
[20] S. Horikoshi, N. Watanabe, H. Onishi, H. Hidaka, N. Serpone, Appl. Catal. B: Environ. 37 (2002) 117–129.
[21] G. Balasubramanian, D.D. Dionysiou, M.T. Suidan, I. Baudin, J.M. Laîné, Appl. Catal. B: Environ. 47 (2004) 73–84.
[22] H. Kozuka, Y. Takahashi, G.L. Zhao, T. Yoko, Thin Solid Films 358 (2000) 172–179.
[23] H. Wang, Z.B. Wu, W.R. Zhao, B.H. Guan, Chemosphere 66 (2007) 185–190.
[24] Z.B. Wu, H. Wang, Y. Liu, Z.L. Gu, J. Hazard. Mater. 151 (2008) 17–25.
[25] G. Balasubramanian, D.D. Dionysiou, M.T. Suidan, V. Subramanian, I. Baudin, J.M. Laîné, J. Mater. Sci. 38 (2003) 823–831.
[26] M. Keshmiri, M. Mohseni, T. Troczynski, Appl. Catal. B: Environ. 53 (2004) 209–219.
[27] J. Medina-Valtierra, J. García-Servín, C. Frausto-Reyes, S. Calixto, Appl. Surf. Sci. 252 (2006) 3600–3608.
[28] Y. Chen, D.D. Dionysiou, Appl. Catal. B: Environ. 62 (2006) 255–264.
[29] Y. Chen, D.D. Dionysiou, J. Mol. Catal. A: Chem. 244 (2006) 73–82.
[30] Y. Chen, D.D. Dionysiou, Appl. Catal. A: Gen. 317 (2007) 129–137.
[31] Y. Chen, D.D. Dionysiou, Appl. Catal. B: Environ. 80 (2008) 147–155.
[32] S.J. Gregg, K.S.W. Sing, Adsorption Surface Area and Porosity, 2nd ed., Academic Press Inc., London, 1982.
[33] G.H. Li, L. Chen, M.E. Graham, K.A. Gray, J. Mol. Catal. A: Chem. 275 (2007) 30–35.
[34] D.C. Hurum, A.G. Agrios, K.A. Gray, T. Rajh, M.C. Thurnauer, J. Phys. Chem. B 107 (2003) 4545–4549.
[35] G. Marcì, V. Augugliaro, M.J. López-Muñoz, C. Martín, L. Palmisano, V. Rives, M. Schiavello, R.J.D. Tilley, A.M. Venezia, J. Phys. Chem. B 105 (2001) 1026–1032.
[36] G. Marcì, V. Augugliaro, M.J. López-Muñoz, C. Martín, L. Palmisano, V. Rives, M. Schiavello, R.J.D. Tilley, A.M. Venezia, J. Phys. Chem. B 105 (2001) 1033–1040.
[37] M. Devadas, O. Kröcher, M. Elsener, A. Wokaun, N. Söger, M. Pfeifer, Y. Demel, L. Mussmann, Appl. Catal. B: Environ. 67 (2006) 187–196.